J Mater Sci (2009) 44:5990–5997
DOI 10.1007/s10853-009-3858-0

INTERFACE SCIENCE

Wetting and interfacial behavior of Ni–Si alloy on different substrates

G. W. Liu · F. Valenza · M. L. Muolo · G. J. Qiao · A. Passerone

Received: 29 June 2009 / Accepted: 27 August 2009 / Published online: 10 September 2009

Abstract Wetting of molten Ni–56 at.% Si alloy on different substrates (SiC ceramic, Ni- and Co-based superalloys, Kovar, and Mo) are performed under different experimental conditions by the sessile drop technique. Temperature, atmosphere, and substrate composition play the key roles in determining the wettability, the spreading characteristics, and the interfacial morphology of the final interfaces. The non-reactive wetting characteristics in Ni–Si/SiC system are confirmed, with a spreading rate increasing with temperature increasing. In the Ni–Si/metal systems the spreading process is determined by the competition between spreading along the substrate surface and the interfacial interactions. Excellent wettability and fast spreading are found in the Ni–Si/Co-based superalloy, Ni–Si/Kovar, and Ni–Si/Mo systems at both the temperatures (1100 and 1200 °C). These results can be used as a reference guide for joining SiC to these metallic components, or to itself, using the Ni–Si alloy as filler metal.

Introduction

Ceramic/metal joining is of great technological significance because, through this process, the individual characteristics of the two types of materials can be used to produce new materials with improved performances. Liquid phase bonding process, including brazing and transient liquid phase bonding (TLPB) technique, is one of the most promising techniques for joining ceramics to metals. Therefore, investigations of wetting, spreading, and interfacial behavior in metal/ceramic [1–11] or metal/metal system [12–16], joining processes and joint performances [17–27] are essential.

Ni- or Co-based superalloys have been and will be increasingly utilized in aeronautical, aerospace, chemical, petrochemical, marine, and energy applications (nuclear, gas turbines, etc.) due to their excellent high temperature strength and excellent oxidation resistance [28, 29]. SiC materials, including those composites using SiC as the matrix, such as SiC_f/SiC, show good overall chemical, thermal, and mechanical properties, which make them suitable candidate materials for aggressive environments. A case in point is nuclear applications, with demands in thermal shock resistance, radiation stability, and low neutron-induced activation [30–32]. Therefore, joining of SiC to superalloys by using high temperature liquid phase bonding techniques, can lead to optimized highly performing applications.

At present, there are still some problems in the SiC/superalloy joining, such as the large thermal residual stresses and excessive interfacial reactions, resulting in the formation of cracks and invalidation of joint, so that it is very important to work on the technological and structural improvements or design of joints. Therefore, many researchers endeavored to seek for some non-reactive joining processes of SiC using binary or ternary alloys with high silicon content for brazing alloys [33–39]. This is attributed to the good non-reactive wettability of these alloys on SiC. Actually, many investigations showed that a series of binary silicon alloys, such as Ni–Si [40–42], Co–Si [43], Fe–Si [44], Au–Si [45, 46], Ag–Si [47, 48], and Cu–Si [49–51], have this good non-reactive wettability in contact with SiC. In addition, Leon et al. [52]

G. W. Liu (✉) · F. Valenza · M. L. Muolo · A. Passerone
Institute for Energetics and Interphases, IENI-CNR,
Via De Marini 6, 16149 Genoa, Italy
e-mail: g.liu@ge.ieni.cnr.it; lgwniat@yahoo.com.cn

G. W. Liu · G. J. Qiao
State Key Laboratory for Mechanical Behavior of Materials,
Xi'an Jiaotong University, Xi'an 710049, China

investigated the influence of Cu coating on the spreading kinetics and equilibrium contact angles of aluminum on SiC for improved the wettability, and argued that the presence of the copper coating at the interface delayed the reactivity of SiC with Al resulting in a clean interface.

The present study is a part of a program aimed at realizing effective SiC/superalloy or SiC/SiC joints using a composite joining technique. The wetting, spreading characteristics, and interfacial behavior of Ni–56Si in contact with SiC, three superalloys, a low thermal expansion coefficient alloy (Kovar) and pure Mo metal are investigated and analyzed. Kovar and Mo, due to their low thermal expansion coefficient and good performances, can be used not only as the other metallic component of the joint but also as the interlayer materials for joining SiC to SiC or superalloys [53].

Experimental process

Materials

A commercial Ni–56Si (all compositions are given in at.%) atomized powder (Goodfellow, England) was used. The Ni–Si alloy was prepared by melting the commercial powder at 1100 °C for 900 s under a vacuum of $\sim 3 \times 10^{-4}$ Pa. A SiC ceramic, two Ni-based superalloys (CMSX486, IN738LC), a Co-based superalloy (ECY768), a low thermal expansion alloy (Kovar 4J32) and pure Mo were used as substrates in wetting experiments. SiC ceramic and alloy disks (Ø15 mm × 2 mm) and Mo sheets (25 mm × 25 mm × 100 μm) have been used. The SiC prepared by hot isostatic press (HIP) process by adding 1% Al_2O_3 as sintering aid have a porosity and surface roughness of about 0.5% and 20 nm, respectively. The compositions of the three superalloys are shown in Table 1. The nominal composition of the Kovar alloy is Fe–32Ni–15Co.

Wetting and characterization

Before each wetting experiment, all the substrates were given a final polishing, and carefully ultrasonically cleaned in alcohol, whereas the Ni–Si alloy drops were chemically and ultrasonically cleaned, and then dried. The wetting and spreading kinetics were evaluated by contact angle (and drop dimensions in Ni–Si/SiC system) measurements using the sessile drop technique in conjunction with the ad hoc designed ASTRAView image analysis software [54, 55]. Sessile drop tests were performed at three temperatures (1100, 1200, and 1350 °C) under high vacuum ($3–5 \times 10^{-4}$ Pa) or static atmosphere (10^5 Pa) of Ar + 5% H_2. In these experiments, the measured oxygen partial pressure at the outlet gauge was of the order $P_{O_2} = 10^{-20}$ Pa (at 700 °C) corresponding, taking into account the equilibrium constant for water, to a $P_{O_2} = 10^{-12}$ Pa at 1100 °C and to a $P_{O_2} = 10^{-10}$ Pa at 1200 °C.

In this paper, the contact angle values reported in metal/metal systems are "apparent contact angles"; indeed, the real liquid–solid interface penetrates into the solid metallic substrates. Thus, the equilibrium of the triple line should be described by applying the Neumann triangle rule instead of the Young's equation [56]. However, the apparent contact angles reported here have a "technological" significance to design joining process. The contact angle values are given here with a precision of ±2°.

The solidified sessile drop/substrate couples were cross-sectioned, polished, and observed by optical microscopy (OM) or scanning electron microscopy (SEM) coupled with energy dispersive spectroscopy (EDS) analysis.

Results and discussion

Ni–Si/SiC system

The spreading kinetics of Ni–56Si on SiC at three temperatures (1100, 1200, and 1350 °C) is shown in Fig. 1. The spreading rate in the first, fast spreading stage obviously increases with temperatures increasing (Fig. 1a), According to the changes of drop dimensions (relative base diameter and drop height) and contact angle, the spreading does not reach the contact equilibrium completely at 1200 °C after a holding time of 3500 s, and the contact angle curve can be separated into three parts, I, II, and III

Table 1 Chemical compositions of the three superalloys used as substrates for wetting experiments

Material	Composition (at.%)[a]																	
	Ni	Co	Cr	Ti	W	Ta	C	Al	Zr	B	Mo	Hf	Re	Nb	Fe	Si	Mn	S
CMSX486	Balance	9.68	5.66	0.90	2.87	1.52	0.36	12.95	0.00	0.09	0.45	0.41	0.99	–	–	–	–	–
IN738LC	Balance	8.19	17.29	4.11	0.77	0.53	0.52	7.28	0.02	0.04	1.11	–	–	0.57	0.10	Traces	Traces	Traces
ECY768	10.05	Balance	27.05	0.27	2.34	1.24	3.04	0.47	0.01	0.01	–	–	–	–	0.06	Traces	Traces	Traces

[a] Nominal compositions from suppliers, checked for main elements by EDS

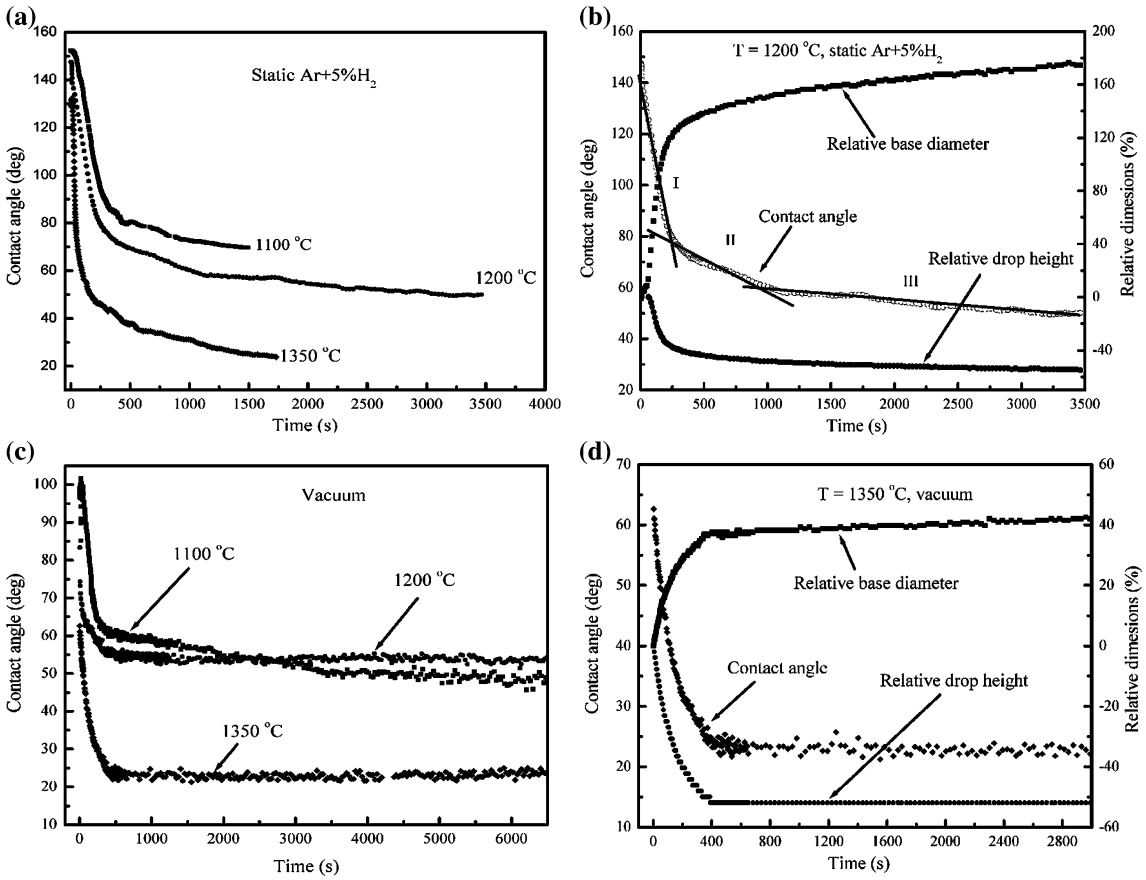

Fig. 1 Contact angle (and relative drop dimensions) as a function of time. Spreading kinetics of Ni–56Si on SiC **a** at three temperatures in static Ar + 5% H_2, **b** at 1200 °C in static Ar + 5% H_2, **c** at three temperatures in a vacuum, and **d** at 1350 °C in a vacuum, showing the effects of temperature and atmosphere on the wettability and spreading process

(Fig. 1b). The spreading rates in the three stages fall in three ranges, namely, $\sim 2.9 \times 10^{-1}$, 2.7×10^{-2}, and $3.7 \times 10^{-3\circ}$ s^{-1}, respectively. As shown in Fig. 1a and c, the spreading processes show some differences between the tests made in a gas mixture (Ar + 5% H_2) and under a vacuum. In vacuum the spreading arrives at the equilibrium in 500 s at 1200 and 1350 °C (Fig. 1c, d), however, at the lower temperature (1100 °C) the spreading does not arrive at the equilibrium after the fast spreading and keeps going at a low rate for ~3000 s (Fig. 1c).

This can be attributed to the fact that the spreading kinetics of silicide/SiC systems can be controlled by the kinetics of removing of wetting barriers (SiO_2 layers) on SiC surface [43, 47]. The related chemical reactions may be expressed as follows:

$$SiO_2\,(s) + Si\,(l) \rightarrow 2SiO\,(g)\uparrow \quad (1)$$

$$SiC\,(s) + 2SiO_2\,(s) \Leftrightarrow 3SiO\,(g)\uparrow + CO\,(g)\uparrow \quad (2)$$

Both reactions imply the presence of gaseous products, so that they are kinetically favoured by vacuum conditions.

Both the contact angles at 1350 °C in static Ar + 5% H_2 and in a vacuum are 23°. The Ni–Si/SiC system has been studied by other authors. In the Ref. [40] a contact angle of 36° was obtained for Ni–47.3Si in contact with highly dense sintered α-SiC at 1500 °C for 1200 s in flowing Ar atmosphere. In other studies [41, 42], four steady contact angles of about 20°–30° were acquired in Ni–Si alloys with $X_{Si} \approx 0.4$–0.85 on 6H–SiC at 1360 °C, in good agreement with our results at 1350 °C.

Figure 2 shows the SEM micrographs of cross-sectioned Ni–Si/SiC couples at two temperatures. It can be seen that the solid–liquid interface in the Ni–56Si/SiC system is smooth and clean without any precipitates also in the region close to the triple line. The same results have been found in the Ni–40Si/SiC [41], Co–72.5Si/SiC [43], and Ag–5Si/SiC systems [47]. This phenomenon has been explained using thermodynamic considerations and the ternary Ni–Si–C diagram [41]. Indeed, when the original content of Si on Ni is above ~40%, the equilibrium is established between the Ni–Si alloy and SiC. After a small dissolution of SiC (difficult to detect in our experiments)

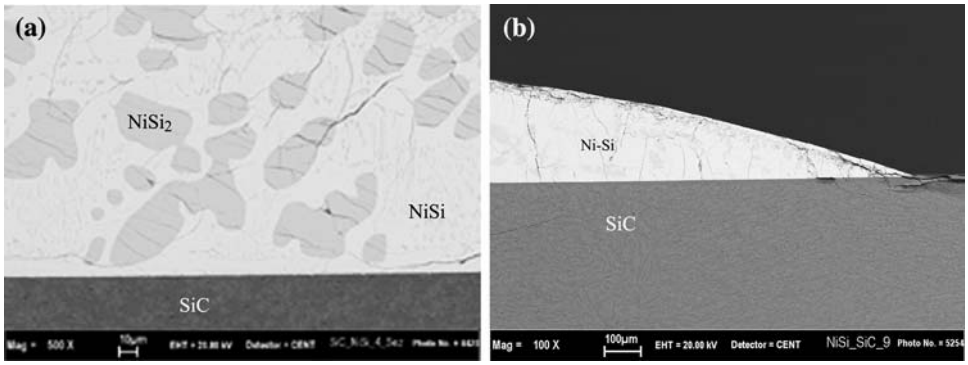

Fig. 2 Cross-section SEM micrographs of the Ni–Si/SiC couples at **a** 1100 °C and **b** 1350 °C, showing the non-reactive wetting characteristics and some cracks formed during cooling. The *white* and *gray* phases in the drop are NiSi and $NiSi_2$, respectively

the saturated liquid alloy does not react anymore with the solid substrate, leaving an undisturbed interface. According to the EDS analysis, the two white and gray phases are NiSi and $NiSi_2$, respectively. Some cracks are present at the interfaces and in the bulk phases due to the presence of the brittle silicides (NiSi and $NiSi_2$) and to the thermal expansion coefficient difference between the Ni–Si alloy and SiC. In addition, the cooling rate also has a great influence on the formation of cracks.

Ni–Si/superalloy systems

The wetting data of Ni–56Si/metal couples are listed in Table 2.

The spreading kinetics of Ni–Si/Ni-based superalloy systems at two temperatures (1100 and 1200 °C) are shown in Fig. 3. The cross-section microstructures of Ni–Si/CMSX486 and Ni–Si/IN738LC couples are shown in Figs. 4 and 5, respectively.

The spreading of Ni–Si/CMSX486 system arrives at a contact angle of ~44° in the first 100 s at 1100 °C, and then the contact angle slowly decreases in the subsequent 800 s to reach ~40° due to limited interfacial diffusion and reaction (Fig. 3). Three layers (A, B, and C) form between the drop and CMSX486 (Fig. 4a, b), with thicknesses of ~500, 100, and 25 μm, respectively. According

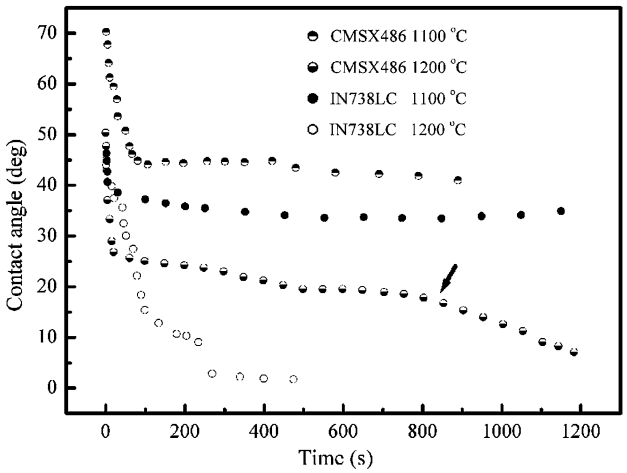

Fig. 3 Contact angles as a function of time. Spreading kinetics of Ni–56Si on two Ni-based superalloys (CMSX486 and IN738LC) at 1100 and 1200 °C

to the EDS analysis, Al, Co, and Cr originated from the substrate enter into the whole drop, while silicon is present in all the three layers. The contents of silicon in layers A and B are almost identical (~35–38%) to that in the solidified drop, while a much lower content of Si (~25%) is found in layer C. At 1200 °C the drop first spreads rapidly in the first 20 s, and then its shape changes slowly

Table 2 Wetting data of the Ni–56Si/metal systems

Substrate	Temperature (°C)	Holding time (s)	Atmosphere	t_F or time while $\theta \leq 10°$ (s)	Final contact angle θ_F (°)
CMSX486	1100	900	Ar + 5% H_2	900	41
CMSX486	1200	1220	Vacuum	1050	<10
IN738LC	1100	1220	Vacuum	550	35
IN738LC	1200	600	Ar + 5% H_2	200	→0
ECY768	1100	300	Vacuum	12	→0
ECY768	1200	300	Vacuum	10	→0
Kovar	1100	1200	Vacuum	15	→0
Kovar	1200	1200	Vacuum	5	→0
Mo	1100	300	Vacuum	15	→0
Mo	1200	300	Vacuum	12	→0

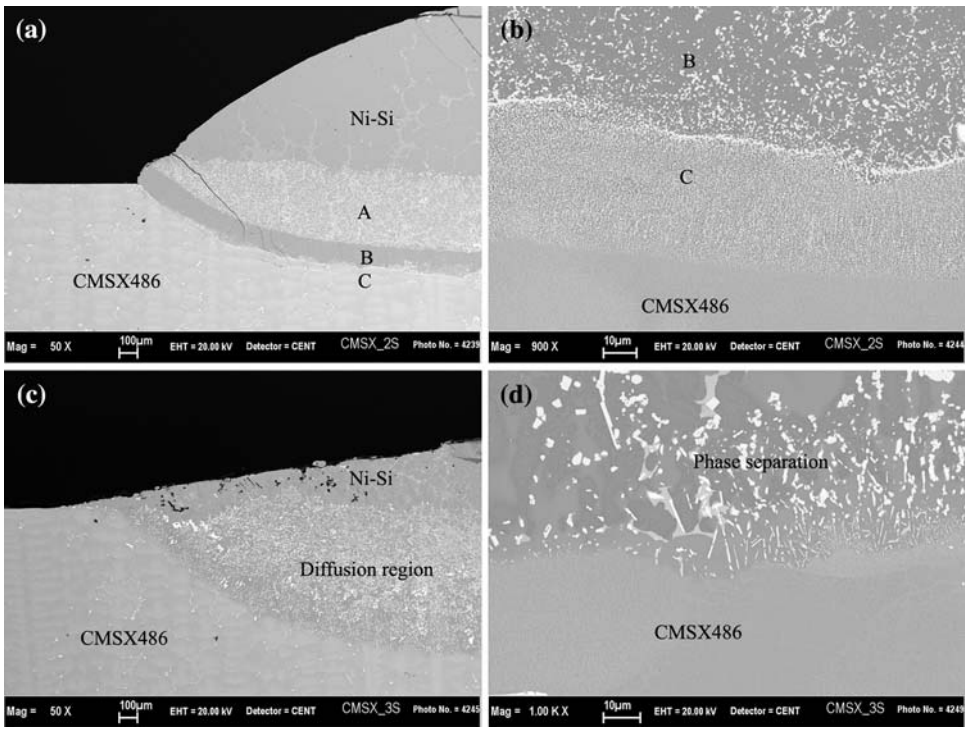

Fig. 4 Cross-section SEM micrographs of the Ni–Si/CMSX486 couple at different temperatures: **a**, **b** 1100 °C; **c**, **d** 1200 °C, showing the difference of wettability and interfacial interactions

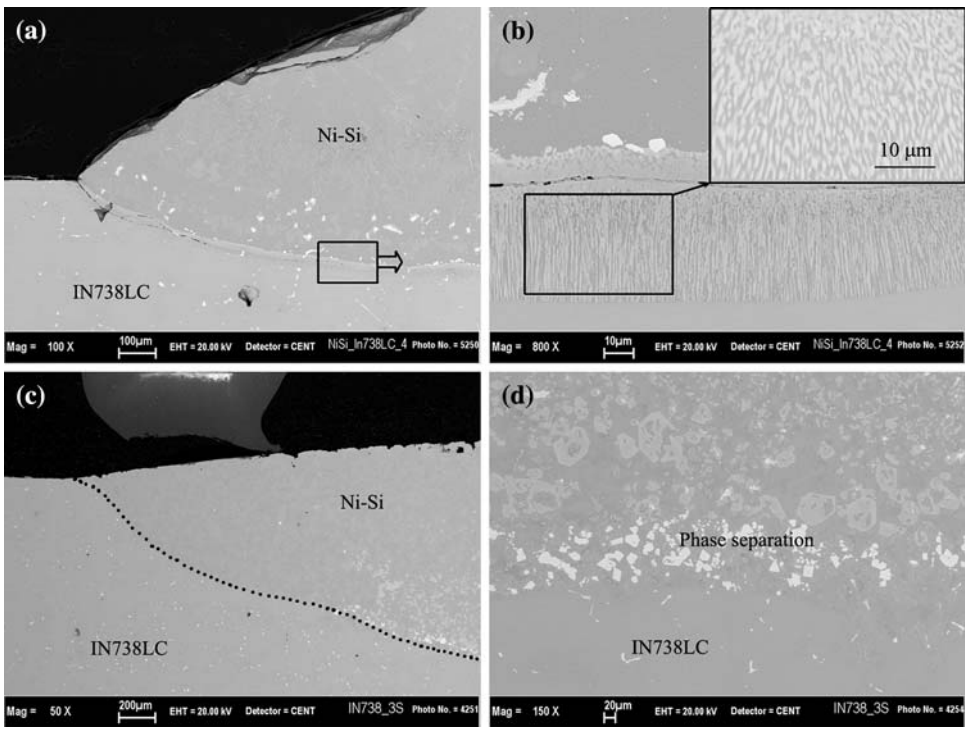

Fig. 5 Cross-section SEM micrographs of the Ni–Si/IN738LC couple at different temperatures **a**, **b** 1100 °C; **c**, **d** 1200 °C, showing the difference of wettability and interfacial interactions. The *dash line* in **c** shows the Ni–Si/IN738LC interface

with time. The contact angle decreases again to <10° at a rate of $\sim 3.3\times10^{-2\circ}$ s^{-1} after the slow spreading period (arrow in Fig. 3): this can be attributed to increasing mutual interactions at the interface during the holding time (Fig. 4c, d). At variance with the previous case, a thick region (diffusion region) is formed by interfacial interactions (diffusion, solution, reaction, and separation). The microstructure of the triple line shows that a competition exists between the strong interfacial interactions and drop spreading along the substrate surface. Similarly, Al, Co,

and Cr enter into the drop, and silicon diffuses into the superalloy substrate up to the diffusion region/substrate interface.

The spreading of the Ni–Si alloy in contact with IN738LC at 1100 °C is similar to that of the Ni–Si/CMSX486 couple. The contact angle falls quickly down to 40° in 5 s, and then decreases slowly to 33°. But subsequently, a small increase of the order of ~2° takes place (Fig. 3). A fiber-like layer ~40 μm thick (with the length of short "fiber" of ~3 μm) emerges at the drop/substrate interface. Some white dots (Fig. 5a, b), also found around the layer, are rich in alloying elements with high melting point, such as Ti, W, and Ta. At 1200 °C the contact angle falls from over 40° down to 20° and 10° in 100 and 200 s, respectively, and then the drop spreads entirely with a contact angle close to 0° (Fig. 3). As shown in Figs. 4c and 5c, there are great similarities in the cross-section microstructures between the Ni–Si/CMSX486 and the Ni–Si/IN738LC couples at 1200 °C. However, a difference exists in the size of segregated high temperature phases (white phases) in the diffusion region.

The cross-section micrographs of Ni–Si/Co-based superalloy (ECY768) couple at 1100 and 1200 °C are shown in Fig. 6. The wettability and spreading characteristics of the Ni–Si/Co-based superalloy system greatly differ from those of the Ni–Si/Ni-based superalloy systems. The spreading in the Ni–Si/ECY768 couple is completed in 15 s with a final contact angle close to 0° at both temperatures, and the drops almost spread all over the substrate surface. This means that spreading dominates in the competition between spreading along the substrate surface and the interfacial interactions (diffusion, dissolution, and reaction) in the drop/substrate system. In addition, the microstructures of the Ni–Si/ECY768 system vary greatly due to the different experimental temperatures. In this case, silicon from the drop diffuses towards the drop/substrate interface during wetting, while Co and Cr, with high concentration (high activity) in the substrate, diffuse first into the drop; however, those high temperature elements in the substrate, such as Ta and W, enter into the drop to a limited extent due to their lower mobility. As a result, a darker layer containing Si, Co, Ni, and Cr forms at the interface (Fig. 6a). However, at higher temperature (1200 °C) all the elements originated from the substrate and drop interdiffuse faster into each other, especially a large amount of Ta and W diffuse into the drop, as shown by the large number of white phases in the drop (Fig. 6b).

Ni–Si/Kovar system

A cross-section micrograph of Ni–Si/Kovar couple at 1200 °C is shown in Fig. 7. The spreading process in Ni–Si/Kovar system is similar to that of Ni–Si/Co-based superalloy (ECY768) system. The liquid drops spread rapidly with a final contact angle of <10° (or close to 0°) in 5 and 15 s at 1100 and 1200 °C, respectively (Table 2). However, the liquid Ni–Si alloy drops can not cover the entire Kovar surface, but present irregular shapes, resulting from strong interfacial interactions between Ni–56Si and Kovar. Furthermore, the extent of interfacial interactions in Ni–Si/Kovar system is very different at the two

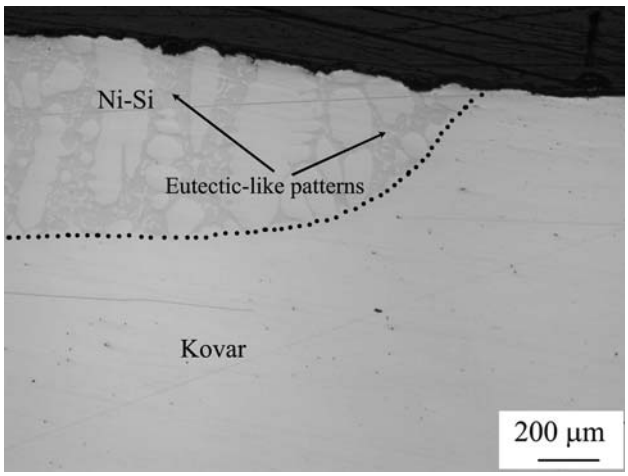

Fig. 7 Cross-section OM micrographs of Ni–Si/Kovar couple at 1200°, showing the eutectic-like patterns in the solidified drop. The *dash line* shows the Ni–Si/Kovar interface

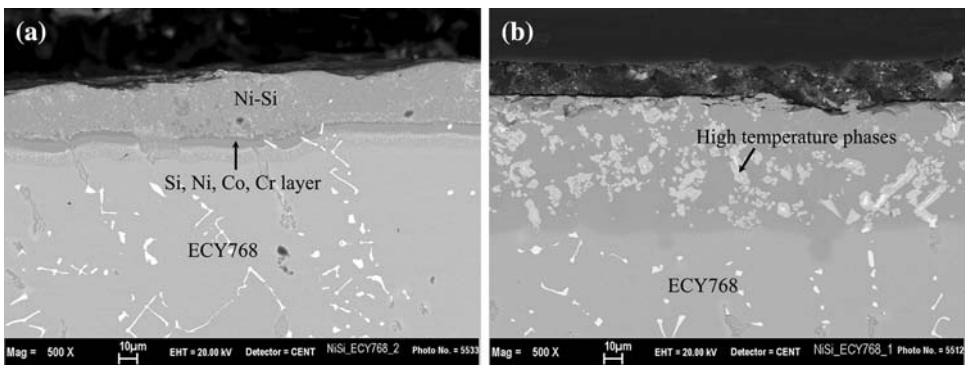

Fig. 6 Cross-section SEM micrographs of Ni–Si/Co-based superalloy (ECY768) couple at **a** 1100 °C and **b** 1200 °C, showing the difference of the morphology in the solidified drop and at the interface

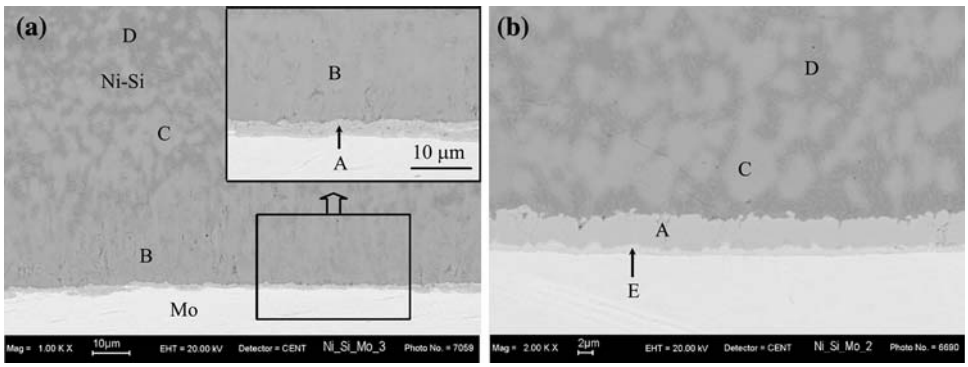

Fig. 8 Cross-section SEM micrographs of the Ni–Si/Mo couple at **a** 1100 °C and **b** 1200 °C, showing the difference of the morphology at the interface

temperatures. At the lower temperature (1100 °C), four elements (Ni, Si, Fe, and Co) distribute evenly in the drop. However, in specimens heated at 1200 °C some observable eutectic-like patterns appear in the drop, larger amounts of Fe and Co diffuse into the drop, and Ni and Si concentrate in the eutectic-like region according to the EDS analysis (Fig. 7).

Ni–Si/Mo system

Similarly to the two previous cases, the spreading of Ni–Si/Mo system at the two temperatures is completed in 15 s and the final contact angle is close to 0° due to the strong mutual interactions in the drop/substrate couple. Figure 8 shows the cross-section micrographs of the Ni–Si/Mo couples. The compositions of the drop and of the interfacial layers are listed in Table 3. As shown in Fig. 8 and Table 3, at the lower temperature (1100 °C) one interfacial layer A (~3 μm) and one gray zone B (~15 μm) exist at the interface (Fig. 8a). However, a double-layer structure (the two layers, A and E, with thicknesses of ~1.5 and 5 μm, respectively) forms at the Ni–Si/Mo interface at 1200 °C (Fig. 8b). The single interfacial layer A corresponds to the thicker one A in the double-layer structure according to the EDS analysis. This can be attributed to the increase of interfacial interactions with temperature increasing. Moreover, the compositions of the two phases (gray-C and dark-D in Fig. 8a, b) in the two specimens are more or less equivalent, respectively.

Table 3 Compositions of the drop and of the interfacial layers in Ni–Si/Mo system

Position	Elemental composition (at.%)					
	1100 °C			1200 °C		
	Ni	Si	Mo	Ni	Si	Mo
Layer A	27.2	34.3	38.5	2.0	32.0	66.0
Zone B	0.9	63.3	35.8			
Gray phase C	1.5	63.3	35.2	1.2	63.8	35.0
Dark phase D	59.4	40.6	0	59.2	40.8	0
Layer E				29.7	33.2	37.1

Conclusions

This study confirms that between 1100 and 1350 °C, the Ni–56Si/SiC system has a non-reactive wetting behavior.

For the Ni–Si/Ni-based superalloy systems, the final contact angles of the Ni–Si alloy in contact with CMSX486 and IN738LC are over 40° and 30° at 1100 °C, however, at 1200 °C they are less than 10° or close to 0°, respectively. A three-layer structure and a fiber-like layer form at the respective drop/substrate interfaces.

For Ni–Si/ECY768, Ni–Si/Kovar, and Ni–Si/Mo systems, all the liquid drops entirely spread in a few seconds (≤15 s) with final contact angles close to 0° at 1100 and 1200 °C (Table 2). The liquid drops almost spread over the whole Co-based superalloy (ECY768) surfaces, at variance with Ni–Si/Kovar system, where a strong competition exists between spreading and interfacial interactions. In Ni–Si/ECY768 system, spreading is much faster than the interaction/diffusion phenomenon. In addition, there are great differences in the morphology in the bulk drop and at the interface due to the difference of substrate compositions and experimental temperature.

Therefore, it can be concluded that temperature, atmosphere, and substrate composition play the key roles in determining the wettability, the spreading characteristics, and the morphology in the drop and at the interface. The spreading process is determined by the competition between spreading along the substrate surface and the interfacial interactions in the Ni–Si/metal systems, and, in particular, the spreading in the Ni–Si/ECY768 system dominates over the solid–liquid interactions. Excellent wettability and fast spreading exist in the Ni–56Si/Co-based superalloy, the Ni–56Si/Kovar, and the Ni–56Si/Mo systems at both the temperatures (1100 and 1200 °C).

Studies on the utilization of the Ni–Si as filler metal and Mo as interlayer to produce SiC/superalloy joints are currently under way in our laboratories.

Acknowledgements The authors wish to thank Mr. Carlo Bottino (IENI) for his skilful and passionate work with SEM and EDS and Mr. Francesco Mocellin (IENI) for technical support.

References

1. Eustathopoulos N (2005) Curr Opin Solid State Mater Sci 9:152
2. Naidich Y (2005) Curr Opin Solid State Mater Sci 9:161
3. Saiz E, Tomsia AP (2005) Curr Opin Solid State Mater Sci 9:167
4. Sobczak N, Singh M, Asthana R (2005) Curr Opin Solid State Mater Sci 9:241
5. Saiz E, Tomsia AP (2004) Nature Mater 3:903
6. Eustathopoulos N, Nicholas MG, Drevet B (1999) Wettability at high temperature. Elsevier, Amsterdam
7. Passerone A, Muolo ML, Valenza F, Monteverde F, Sobczak N (2009) Acta Mater 75:356
8. Muolo ML, Ferrera E, Novakovic R, Passerone A (2003) Scr Mater 48:191
9. Passerone A, Muolo ML, Passerone D (2006) J Mater Sci 41:5088. doi:10.1007/s10853-006-0442-8
10. Naidich YV, Zhuravlev VS, Gab II, Kostyuk BD, Krasovskyy VP, Adamovskyy AA, Taranets NY (2008) J Eur Ceram Soc 28:717
11. Bougiouri V, Voytovych R, Dezellus O, Eustathopoulos N (2007) J Mater Sci 42:2016. doi:10.1007/s10853-006-1483-8
12. Aluru R, Gale WF, Chitti SV, Sofyan N, Love RD, Fergus JW (2008) Mater Sci Technol 24:517
13. Ma GF, Zhang HL, Zhang HF, Li H, Hu ZQ (2008) J Alloys Compd 464:248
14. Xu J, Liu X, Bright MA, Hemrick JG, Sikka V, Barbero E (2008) Metall Mater Trans A 39A:1382
15. Brochu M, Pugh M, Drew RAL (2004) Intermetallics 12:289
16. Gauffier A, Saiz E, Tomsia AP, Hou PY (2007) J Mater Sci 46:9524. doi:10.1007/s10853-007-2093-9
17. Xiong HP, Mao W, Xie YH, Chen B, Guo WL, Li XH, Cheng YY (2007) J Mater Res 22:2727
18. Xiong HP, Mao W, Xie YH, Chen B, Guo WL, Li XH, Cheng YY (2007) Mater Lett 61:4662
19. Prakash P, Mohandas T, Raju PD (2005) Scr Mater 52:1169
20. Chen B, Xiong HP, Mao W, Guo WL, Cheng YY, Li XH (2007) Acta Metall Sin 43:1181
21. Liu GW, Qiao GJ, Wang HJ, Yang JF, Lu TJ (2008) J Eur Ceram Soc 28:2701
22. Liu GW, Li W, Qiao GJ, Wang HJ, Yang JF, Lu TJ (2009) J Alloys Compd 470:163
23. Zhang CG, Qiao GJ, Jin ZH (2002) J Eur Ceram Soc 22:2181
24. Qiao GJ, Zhang CG, Jin ZH (2003) Ceram Int 29:7
25. Hattali ML, Valette S, Ropital F, Mesrati N, Treheux D (2009) J Mater Sci 44:3198. doi:10.1007/s10853-009-3426-7
26. Li SJ, Zhou Y, Duan HP, Qiu JH, Zhang Y (2003) J Mater Sci 38:4065. doi:10.1023/A:1026135220737
27. Shalz ML, Dalgleish BJ, Tomsia AP, Glaeser AM (1993) J Mater Sci 28:1673. doi:10.1007/BF00363367
28. Tan L, Sridharan K, Allen TR (2007) J Nucl Mater 371:171
29. Kumar A, Rajkumar KV, Jayakumar T, Raj B, Mishra B (2006) J Nucl Mater 350:284
30. Jones RH, Giancarli L, Hasegawa A, Katoh Y, Kohyama A, Riccardi B, Snead LL, Weber WJ (2002) J Nucl Mater 307:1057
31. Riccardi B, Giancarli L, Hasegawa A, Katoh Y, Kohyama A, Jones RH, Snead LL (2004) J Nucl Mater 329:56
32. Ferraris M, Salvo M, Casalegno V, Ciampichetti A, Smeacetto F, Zucchetti M (2008) J Nucl Mater 375:410
33. Mcdermid JR, Drew RAL (1991) J Am Ceram Soc 74:1855
34. Koltsov A, Hodaj F, Eustathopoulos N (2008) Mater Sci Eng A 495:259
35. Riccardi B, Nannetti CA, Woltersdorf J, Pippel E, Petrisor T (2004) Int J Mater Prod Technol 20:440
36. Riccardi B, Nannetti CA, Woltersdorf J, Pippel E, Petrisor T (2002) J Mater Sci 37:5029. doi:10.1023/A:1021087632155
37. Riccardi B, Nannetti CA, Petrisor T, Woltersdorf J, Pippel E, Libera S, Pillonni L (2004) J Nucl Mater 329:562
38. Riccardi B, Nannetti CA, Petrisor T, Sacchetti M (2004) J Nucl Mater 307:1237
39. Li JK, Liu L, Wu YT, Zhang WL, Hu WB (2008) Mater Lett 62:3135
40. Tsoga A, Ladas S, Nikolopoulos P (1997) Acta Mater 45:3515
41. Rado C, Kalogeropoulou S, Eustathopoulos N (1999) Acta Mater 47:461
42. Rado C, Kalogeropoulou S, Eustathopoulos N (2000) Scr Mater 42:203
43. Mailliart O, Hodaj F, Chaumat V, Eustathopoulos N (2008) Mater Sci Eng A 495:174
44. Kalogeropoulou S, Baud L, Eustathopoulos N (1995) Acta Metall Mater 43:907
45. Drevet B, Kalogeropoulou S, Eustathopoulos N (1993) Acta Mater 41:3119
46. Naidich YV, Zhuravlev V, Krasovskaya N (1998) Mater Sci Eng A 245:293
47. Rado C, Kalogeropoulou S, Eustathopoulos N (2000) Mater Sci Eng A 276:195
48. Li JG (1994) Mater Lett 18:291
49. Gasse A, Chaumat G, Rado C, Eustathopoulos N (1996) J Mater Sci Lett 15:1630
50. Landry K, Rado C, Eustathopoulos N (1996) Metall Mater Trans A 27:3181
51. Rado C, Eustathopoulos N (2004) Interface Sci 12:85
52. Leon CA, Mendoza-Suarez G, Drew RAL (2006) J Mater Sci 41:5081. doi:10.1007/s10853-006-0443-7
53. Liu GW, Qiao GJ, Valenza F, Muolo ML, Passerone A (2009) Mater Sci Eng A (submitted)
54. Liggieri L, Passerone A (1989) High Temp Technol 7:82
55. Passerone A, Ricci E (1998) In: Möbius D, Miller R (eds) Drops and bubbles in interfacial research. Elsevier, Amsterdam
56. Defay R, Prigogine I, Bellemans A, Everett DH (1966) Surface tension and adsorption. Logmans, London